Physics of the Solid State, Vol. 43, No. 12, 2001, pp. 2290–2300. Translated from Fizika Tverdogo Tela, Vol. 43, No. 12, 2001, pp. 2198–2208.

LATTICE DYNAMICS AND PHASE TRANSITIONS

Lattice Dynamics and Statistical Mechanics of the $Fm3m \longrightarrow I4/m$ Structural Phase Transition in Rb_2KInF_6

V. I. Zinenko and N. G. Zamkova

Kirensky Institute of Physics, Siberian Division, Russian Academy of Sciences, Akademgorodok, Krasnoyarsk, 660036 Russia

e-mail: zvi@iph.krasn.ru

Received May 7, 2001

Abstract—The static and dynamic properties of cubic Rb_2KInF_6 crystals with elpasolite structure are calculated using a nonempirical method. Calculations are performed within a microscopic ionic-crystal model taking into account the deformation and polarization of ions. The deformation parameters of ions are determined by minimizing the total energy of the crystal. The calculated equilibrium lattice parameters agree satisfactorily with the experimental data. It is found that in the cubic phase there are vibrational modes that are unstable everywhere in the Brillouin zone. The eigenvectors of the unstablest mode at the center of the Brillouin zone of the cubic phase are associated with the displacements of F ions and correspond to rotations of InF_6 octahedra. Condensation of this mode leads to a tetragonal distortion of the structure. In order to describe the $Fm3m \longrightarrow I4/m$ phase transition, an effective Hamiltonian is constructed under the assumption that the soft mode whose eigenvector corresponds to octahedron rotation is local and coupled with homogeneous elastic strains. The parameters of the effective Hamiltonian are determined using the calculated crystal energy for the distorted structures due to soft-mode condensation. The thermodynamic properties of the system with this model Hamiltonian are investigated using the Monte Carlo method. The phase transition temperature is calculated to be 550 K, which is twice its experimental value (283 K). The tetragonal phase remains stable down to $T = 0$ K; the effective Hamiltonian used in this paper thus fails to describe the second phase transition (to the monoclinic phase). Thus, the transition to the tetragonal phase occurs for the most part through octahedron rotations; however, additional degrees of freedom, first of all, the displacements of Rb ions, should be included into the effective Hamiltonian in order to describe the transition to the monoclinic phase. © *2001 MAIK "Nauka/Interperiodica".*

1. INTRODUCTION

Halides with the elpasolite structure $A_2BB^{3+}X_6$ undergo a wide variety of structural phase transitions associated with lattice instability in the high-symmetry cubic phase. In the lower temperature phases, these compounds show either homogeneous nonpolar distortions of the lattice or distortions that are accompanied by a change in the unit-cell volume of the crystal. In most crystals of this family, structural distortions are associated either with rotations of the octahedra $B^{3+}X_6$ or with a combination of octahedron rotations and *A*-atom displacements.

Instability of the crystal lattice against normal vibrations involving octahedron rotations is likely a characteristic feature of perovskite-like compounds. In most halides and some oxides with perovskite structure, this instability leads to structural phase transitions to a lower symmetry phase, which are accompanied by an increase in the unit-cell volume in comparison with that of the initial cubic phase.

The problem of instability of the perovskite structure against distortions corresponding either to the ferroelectric lattice vibration mode or to octahedron rotations has been discussed in experimental and theoretical studies for several decades. In recent years, many papers have been published in which, using the density-functional method, the electronic band structure and lattice vibration frequencies were calculated and the statistical mechanics of phase transitions for some perovskites were considered. Those calculations have given some insight into the source of crystal lattice instability and the nature of ferroelectricity and antiferroelectricity in oxides with perovskite structure (see, e.g., [1–4]).

For crystals with elpasolite structure, scarcely any calculations of the crystal lattice vibration spectrum exist. At the same time, these crystals have been intensely studied experimentally using various methods and, at the present time, there do exist data on the structures of the low-symmetry phases, physical properties, and the effect of phase transitions on them for many of these crystals (see, e.g., the recent review [5]).

The Rb_2KInF_6 crystal belongs to the elpasolite family; its high-symmetry phase has a cubic crystal structure with one molecule per unit cell (Fig. 1) and belongs to the space group $Fm3m$. As the temperature decreases, Rb_2KInF_6 undergoes two subsequent structural phase transitions: one to a tetragonal phase (space

group $I4/m$) with the same unit-cell volume as that in the cubic phase (at T_{c1}= 283 K) and another to a monoclinic phase (space group $P12_1/n1$) with two molecules per unit cell (at T_{c2}= 264 K). Structural studies of the low-symmetry phases of the isomorphic compound Rb_2KScF_6 have revealed [5] that the distortions of the cubic structure in the tetragonal phase are associated, for the most part, with ScF_6 octahedron rotations, which are homogeneous over the entire crystal. The distortions in the lower temperature monoclinic phase are associated with inhomogeneous rotations of ScF_6 octahedra and with displacements of Rb ions from their equilibrium positions in the tetragonal phase. It should be noted that in the series of isomorphic compounds Rb_2KMF_6 (M = Ga, Sc, In, Lu), the phase transition temperature from the cubic phase increases with the size of the trivalent ion M.

Earlier, we calculated the entire lattice vibration spectra of the Rb_2KScF_6 crystal in the unstable cubic and tetragonal phases and the stable monoclinic phase [6] within the Gordon–Kim model generalized by Ivanov and Maksimov [7] to the case of deformable and polarizable ions. Using an effective Hamiltonian in which the coupling constants were calculated without fitting parameters, we described the $Fm3m \longrightarrow I4/m$ phase transition in this compound [8]. The calculated phase transition temperature and the physical properties in the vicinity of the phase transition point were found to agree well with the experimental data.

The objective of this paper is to calculate the equilibrium volume, the entire lattice vibration spectrum, and the high-frequency dielectric constant of Rb_2KInF_6 in the cubic phase from first principles and to determine the parameters of the effective Hamiltonian that describes the $Fm3m \longrightarrow I4/m$ phase transition in this compound. We also investigate the thermodynamic properties of the phase transition using the Monte Carlo (MC) method.

In Section 2, we describe the model and the method for calculating the total energy, the frequencies of normal lattice vibrations, the dynamic charges, and the high-frequency dielectric constant. The results from calculations of the lattice dynamics of the Rb_2KInF_6 crystal are presented in Section 3. In Section 4, we discuss the effective Hamiltonian, which includes the minimum number of degrees of freedom (more specifically, the local mode corresponding to InF_6 octahedron rotations) and homogeneous elastic strains and calculate the parameters of the model Hamiltonian. Some details of the investigation of the thermodynamic behavior of the system with this model Hamiltonian (using the Monte Carlo algorithm), as well as the results of calculations and their discussion, are presented in Section 5.

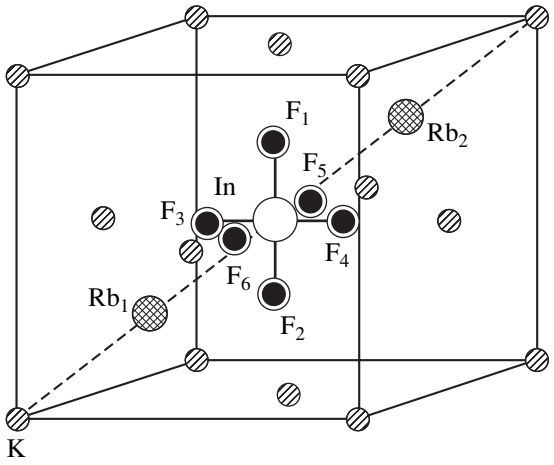

Fig. 1. Crystalline structure of Rb_2KInF_6 in the cubic phase. One molecule and a unit cell of the fcc K lattice are shown. The six Rb ions of the other three molecules are situated at 1/4 and 3/4 lengths of the three other cube body diagonals. The remaining In ions are located at the midpoints of the cube edges. Each In ion is surrounded by six F ions.

2. MODEL AND CALCULATION TECHNIQUE

In order to calculate the lattice vibration spectrum of the $RbKInF_6$ crystal, we use the ionic-crystal model proposed by Ivanov and Maksimov [7]. In this model, the ionic crystal consists of overlapping individual spherically symmetric polarizable ions. The total electronic density of the crystal is written as

$$\rho(\mathbf{r}) = \sum_i \rho_i(\mathbf{r} - \mathbf{R}_i),$$

where summation is carried out over all ions of the crystal. In the density-functional theory, the total crystal energy including only pairwise interaction has the form

$$E_{\text{cr}} = \frac{1}{2}\sum_{i \neq j} \frac{Z_i Z_j}{|\mathbf{R}_i - \mathbf{R}_j|} + \sum_i E_i^{\text{self}}(R_{\text{W}}^i) + \frac{1}{2}\sum_{i \neq j} \Phi_{ij}(R_{\text{W}}^i, R_{\text{W}}^j, |\mathbf{R}_i - \mathbf{R}_j|), \quad (1)$$

where Z_i is the charge of the ith ion,

$$\Phi_{ij}(R_{\text{W}}^i, R_{\text{W}}^j, |\mathbf{R}_i - \mathbf{R}_j|) = E\{\rho_i(\mathbf{r} - \mathbf{R}_i) + \rho_j(\mathbf{r} - \mathbf{R}_j)\} - E\{\rho(\mathbf{r} - \mathbf{R}_i)\} - E\{\rho(\mathbf{r} - \mathbf{R}_j)\}, \quad (2)$$

the energy $E\{\rho\}$ is calculated using the density-functional method and the local approximation to the kinetic and exchange-correlation energies, and $E_i^{\text{self}}(R_{\text{W}}^i)$ is the self-energy of the ion. The electronic density of an individual ion and its self-energy are cal-

Table 1. Calculated and experimental [11] atomic coordinates and lattice parameters

Atom	Position	Occupancy	a_0 = 8.84 Å			a_{exp} = 9.10 Å		
			x/a_0	y/a_0	z/a_0	x/a_{exp}	y/a_{exp}	z/a_{exp}
Rb	8*c*	1	0.25	0.25	0.25	0.25	0.25	0.25
K	4*b*	1	0.50	0.50	0.50	0.50	0.50	0.50
In	4*a*	1	0.0	0.0	0.0	0.0	0.0	0.0
F	24*e*	1	0.23	0.0	0.0	0.222	0.0	0.0

culated using the crystal potential as approximated by a charged sphere (the Watson sphere):

$$V(r) = \begin{cases} Z_i^{\text{ion}}/R_W & r < R_W \\ Z_i^{\text{ion}}/r & r > R_W, \end{cases}$$

where R_W is the radius of the Watson sphere. The radii R_W^i for individual ions are found by minimizing the total energy of the crystal. When calculating the lattice dynamics, the terms describing the changes in energy due to the displacements of ions from their equilibrium positions should be included in the crystal energy in Eq. (2). The dynamic matrix which includes the electronic polarization of the ions and the ionic deformation caused by the crystal field for crystals of arbitrary symmetry in the model used here is written out in [9]. In calculating the lattice vibration frequencies of Rb_2KInF_6 and when classifying the vibrational modes by their symmetry, we use the results of [9].

The Coulomb interaction contribution to the dynamic matrix is calculated using the Ewald method. The ionic parameters are determined using the algorithm developed by Liberman *et al.* [10]. The pairwise interaction energy in Eq. (2) and the ionic polarizability are calculated using the technique developed by Ivanov and Maksimov [7], with the kinetic energy taken in the Thomas–Fermi approximation and with the exchange-correlation energy calculated in the Hedin–Lundqvist approximation. In calculating the derivatives involved in the dynamic matrix, the dependences of the energy on the distances R and the Watson sphere potentials V are approximated by Chebyshev polynomials.

Table 2. Ionic polarizabilities, high-frequency dielectric constants, and dynamic charges

Atom	ε_∞ = 1.86			
	α, Å^3	Z_{xx}	Z_{yy}	Z_{zz}
Rb	1.39	1.24	1.24	1.24
K	0.74	1.17	1.17	1.17
In	0.37	3.02	3.02	3.02
F_1	0.82	–1.03	–1.03	–1.28
F_2	0.82	–1.03	–1.28	–1.03
F_3	0.82	–1.28	–1.03	–1.03

3. LATTICE VIBRATION SPECTRUM

In this section, we present the results of calculations of the equilibrium volume, the dielectric constant, the dynamic charges, and the lattice vibration spectra of the Rb_2KInF_6 crystal in the cubic phase.

The equilibrium lattice parameter and the positions of the atoms in a unit cell were determined by minimizing the total crystal energy as a function of volume. The calculated lattice parameter and coordinates of the ions, as well as their experimental values, are presented in Table 1. It is seen that the calculated values coincide with the experimental values to within 4%. The radii of the Watson spheres for Rb^+, K^+, In^{3+}, and F^- ions found by minimizing the total energy are 2.125, 2.5625, 3.5, and 2.625 a.u., respectively. The calculated values of the polarizabilities of the ions, high-frequency dielectric constant, and dynamic ionic charges of the crystal under study are listed in Table 2.

The calculated dispersion curves of the lattice vibration frequencies of Rb_2KInF_6 in the cubic phase are shown in Fig. 2, and Table 3 lists the limiting vibration frequencies (at $q = 0$) and the frequencies of some Raman-active vibration modes measured in [11]. It can be seen that the calculated limiting frequencies of Raman-active modes are 10–20% lower than the experimental values.

It is also seen from Fig. 2 and Table 3 that there are imaginary vibration frequencies, which is indicative of structural instability of the cubic phase of the crystal. It should be emphasized that unstable modes arise everywhere in the Brillouin zone (BZ) and that their frequencies at symmetry points of the BZ are comparable in absolute value. Since the experimentally observed phase transitions in the Rb_2KInF_6 crystal are associated with instability of vibrational modes at the center and at the boundary point X of the BZ, we will discuss only the vibrational modes at these points. At the center of the BZ, three modes become unstable in the cubic structure. The strongest instability (for which the square of the normal-mode frequency is negative and

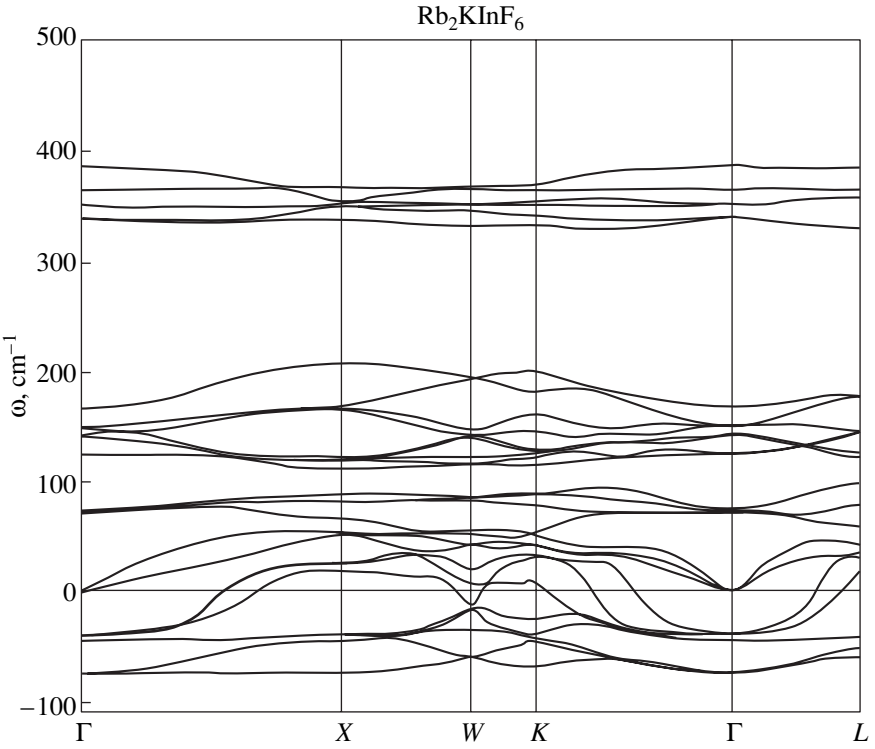

Fig. 2. Dispersion curves of the vibrational modes of the Rb_2KInF_6 crystal in the cubic phase. Negative values correspond to imaginary frequencies.

has a maximum absolute value) is associated with the threefold degenerate T_{1g} mode, in which only four F atoms are displaced from their equilibrium positions [9, 12]. As a result of these displacements, the InF_6 octahedron is rotated as a whole. Another (ferroelectric) unstable mode is the transverse polar mode T_{1u}, in which all atoms in a unit cell are displaced from their equilibrium positions in the cubic phase. However, to our knowledge, ferroelectric phase transitions have not been observed experimentally in halide crystals with elpasolite structure. Finally, the third unstable mode is the threefold degenerate T_{2g} mode. One of the eigenvectors of this mode corresponds to rotation of the InF_6 octahedron about a cube body diagonal and to simultaneous displacements of the Rb atoms situated on this diagonal toward each other. It should be noted that in the vibration spectrum of the crystal under study, there is also a stable mode of the same symmetry, T_{2g} (Table 3).

At point X on the BZ boundary, the strongest lattice instability is associated with the nondegenerate X_2^+ mode, in which the displacements of the four F ions ($F_{3y} = -F_{4y} = F_{5z} = -F_{6z}$) also correspond to rotation of the InF_6 octahedron as a whole. However, the rotations are inhomogeneous over the crystal and condensation of this mode leads to doubling of the unit-cell volume. As indicated in the introduction, when the temperature is decreased, the crystal first undergoes the transition to the tetragonal phase, which is associated with condensation of the soft T_{1g} mode at the center of the BZ.

Table 3. Limiting $q = 0$ vibration frequencies (cm^{-1}) in the cubic phase

ω_i	Cubic phase			
	degeneracy	vibrational mode	frequency	[11]
ω_1	3	T_{1g}	74i	
ω_{2T}	2	T_{1u}	44i	
ω_3	3	T_{2g}	39i	80
ω_4	3	T_{1u}	0	
ω_{2L}	1	T_{1u}	71	
ω_5	3	T_{2u}	74	
ω_{6T}	2	T_{1u}	125	
ω_7	3	T_{2g}	142	210
ω_{6L}	1	T_{1u}	149	
ω_{8T}	2	T_{1u}	149	
ω_{8L}	1	T_{1u}	167	
ω_9	2	E_g	340	380
ω_{11}	1	A_{1g}	365	510
ω_{10T}	2	T_{1u}	352	
ω_{10L}	1	T_{1u}	386	

4. DERIVATION OF THE EFFECTIVE HAMILTONIAN AND CALCULATION OF ITS PARAMETERS

The effective model Hamiltonian in the local-mode approximation [13] has been used in several publications to describe ferroelectric and structural phase transitions in the diatomic compound GeTe [14] and oxides with perovskite structure [1–4]. When deriving the model Hamiltonian, we used the scheme proposed in [3, 4, 14].

In the threefold degenerate T_{1g} vibrational mode at $q = 0$ and the nondegenerate vibrational modes along the lines going through the center of the BZ and one of the points X, Y, or Z on the BZ boundary, only F ions are displaced and their displacements v_k^E in these modes are subject to the relations

$$\begin{aligned} T_{1g}&: \begin{cases} -v_{1y}^F = v_{2y}^F = v_{5z}^F = -v_{6z}^F \\ -v_{1x}^F = v_{2x}^F = -v_{3z}^F = v_{4z}^F \\ -v_{3y}^F = v_{4y}^F = -v_{5x}^F = v_{6x}^F \end{cases} \\ X_3&: -v_{1y}^F = v_{2y}^F = v_{5z}^F = -v_{6z}^F, \\ Y_3&: -v_{1x}^F = v_{2x}^F = -v_{3z}^F = v_{4z}^F, \\ Z_3&: -v_{3y}^F = v_{4y}^F = -v_{5x}^F = v_{6x}^F. \end{aligned} \tag{3}$$

These F-ion displacements lead to rotation of the InF_6 octahedron. We derive the model Hamiltonian in the local-mode approximation and take into account only the modes in Eq. (3); the other modes are assumed to be insignificant in the structural transition from the cubic to the tetragonal phase. Thus, for Rb_2KInF_6, a local mode is assumed to have the form

$$S_\alpha = \frac{1}{a_0}\sum_k \xi_{\alpha k} v_k^F, \tag{4}$$

where $\alpha = x, y, z$; v_k^F is the oscillation amplitude of the kth F ion given by Eq. (3); $\xi_{\alpha k}$ are the eigenvectors of a lattice vibrational mode; and $a_0 = 16.71$ a.u. is the lattice parameter in the cubic phase. The vectors ξ are presented in Table 4.

Under the symmetry operations of the high-symmetry cubic phase, the local mode (S_x, S_y, S_z) is transformed as a pseudovector. Thus, in order to construct the effective Hamiltonian that describes the structural phase transition $Fm3m \longrightarrow I4/m$, we proceed as follows. The three-component local mode (pseudovector) is placed at sites of an fcc lattice. For the sake of simplicity, anharmonicity is taken into account in the effective Hamiltonian only through the single-site potential, which contains all second- and fourth-order terms and some anisotropic terms of the sixth order. Pairwise interaction between the local modes at different sites is included only for the nearest and next-to-nearest neighbor sites. The interaction between the local mode and spatially homogeneous elastic strains is also allowed for. Thus, taking into account the transformation properties of the local mode and the fcc lattice under cubic-symmetry operations, the microscopic model Hamiltonian is written as [8]

$$\begin{aligned} H &= \sum_i (H_i^{\text{anh}} + H_i^{SS}) + H^{Se} + H^{ee}, \\ H_i^{\text{anh}} &= B(S_{ix}^4 + S_{iy}^4 + S_{iz}^4) + C(S_{ix}^2 S_{iy}^2 + S_{iy}^2 S_{iz}^2 + S_{iz}^2 S_{ix}^2) \\ &\quad + D(S_{ix}^6 + S_{iy}^6 + S_{iz}^6), \end{aligned} \tag{5}$$

$$\begin{aligned} H_i^{SS} = S_{ix}\Bigg[& AS_{ix} + a_1 \sum_{\mathbf{d} = (0, \pm 1, \pm 1)} S_x\left(\mathbf{R}_i + \frac{a_0\mathbf{d}}{2}\right) \\ & + a_2 \sum_{\mathbf{d} = \begin{pmatrix} \pm 1, \pm 1, 0 \\ \pm 1, 0, \pm 1 \end{pmatrix}} S_x\left(\mathbf{R}_i + \frac{a_0\mathbf{d}}{2}\right) \\ & + a_3 \sum_{\mathbf{d} = (\pm 1, 0, \pm 1)} (\mathbf{d}\cdot\mathbf{z})(\mathbf{d}\cdot\mathbf{x}) S_z\left(\mathbf{R}_i + \frac{a_0\mathbf{d}}{2}\right) \\ & + a_3 \sum_{\mathbf{d} = (\pm 1, \pm 1, 0)} (\mathbf{d}\cdot\mathbf{y})(\mathbf{d}\cdot\mathbf{x}) S_y\left(\mathbf{R}_i + \frac{a_0\mathbf{d}}{2}\right)\Bigg] \\ & + S_{iy}\Bigg[AS_{iy} + a_1 \sum_{\mathbf{d} = (\pm 1, 0, \pm 1)} S_y\left(\mathbf{R}_i + \frac{a_0\mathbf{d}}{2}\right) \end{aligned}$$

Table 4. Eigenvectors of the threefold degenerate vibrational mode T_{1g}

Components	Rb1	Rb2	F1	F2	F3	F4	F5	F6	K	In
ξ_x	000	000	$0-\frac{1}{2}0$	$0\frac{1}{2}0$	000	000	$00\frac{1}{2}$	$00-\frac{1}{2}$	000	000
ξ_y	000	000	$-\frac{1}{2}00$	$\frac{1}{2}00$	$00-\frac{1}{2}$	$00\frac{1}{2}$	000	000	000	000
ξ_z	000	000	000	000	$0-\frac{1}{2}0$	$0\frac{1}{2}0$	$-\frac{1}{2}00$	$\frac{1}{2}00$	000	000

$$+ a_2 \sum_{\mathbf{d} = \binom{\pm1, \pm1, 0}{0, \pm1, \pm1}} S_y\left(\mathbf{R}_i + \frac{a_0\mathbf{d}}{2}\right)$$

$$+ a_3 \sum_{\mathbf{d} = (0, \pm1, \pm1)} (\mathbf{d}\cdot\mathbf{z})(\mathbf{d}\cdot\mathbf{y}) S_z\left(\mathbf{R}_i + \frac{a_0\mathbf{d}}{2}\right)$$

$$+ a_3 \sum_{\mathbf{d} = (\pm1, \pm1, 0)} (\mathbf{d}\cdot\mathbf{x})(\mathbf{d}\cdot\mathbf{y}) S_x\left(\mathbf{R}_i + \frac{a_0\mathbf{d}}{2}\right)\Bigg]$$

$$+ S_{iz}\Bigg[AS_{iz} + a_1 \sum_{\mathbf{d} = (\pm1, \pm1, 0)} S_z\left(\mathbf{R}_i + \frac{a_0\mathbf{d}}{2}\right)$$

$$+ a_2 \sum_{\mathbf{d} = \binom{\pm1, 0, \pm1}{0, \pm1, \pm1}} S_z\left(\mathbf{R}_i + \frac{a_0\mathbf{d}}{2}\right)$$

$$+ a_3 \sum_{\mathbf{d} = (0, \pm1, \pm1)} (\mathbf{d}\cdot\mathbf{y})(\mathbf{d}\cdot\mathbf{z}) S_x\left(\mathbf{R}_i + \frac{a_0\mathbf{d}}{2}\right)$$

$$+ a_3 \sum_{\mathbf{d} = (\pm1, 0, \pm1)} (\mathbf{d}\cdot\mathbf{x})(\mathbf{d}\cdot\mathbf{z}) S_y\left(\mathbf{R}_i + \frac{a_0\mathbf{d}}{2}\right)\Bigg]$$

$$+ S_{ix}\Bigg[b_1 \sum_{\mathbf{d} = (\pm1, 0, 0)} S_x(\mathbf{R}_i + a_0\mathbf{d})$$

$$+ b_2 \sum_{\mathbf{d} = \binom{0, \pm1, 0}{0, 0, \pm1}} S_x(\mathbf{R}_i + a_0\mathbf{d})\Bigg]$$

$$+ S_{iy}\Bigg[b_1 \sum_{\mathbf{d} = (0, \pm1, 0)} S_y(\mathbf{R}_i + a_0\mathbf{d})$$

$$+ b_2 \sum_{\mathbf{d} = \binom{\pm1, 0, 0}{0, 0, \pm1}} S_y(\mathbf{R}_i + a_0\mathbf{d})\Bigg]$$

$$+ S_{iz}\Bigg[b_1 \sum_{\mathbf{d} = (0, 0, \pm1)} S_z(\mathbf{R}_i + a_0\mathbf{d})$$

$$+ b_2 \sum_{\mathbf{d} = \binom{\pm1, 0, 0}{0, \pm1, 0}} S_z(\mathbf{R}_i + a_0\mathbf{d})\Bigg],$$

$$H^{Se} = \sum_i \Big\{ g_1(e_1 + e_2 + e_3)(S_{ix}^2 + S_{iy}^2 + S_{iz}^2)$$

$$+ g_2\Big[(e_1 + e_2 - 2e_3)(S_{ix}^2 + S_{iy}^2 - 2S_{iz}^2)$$

$$+ 3(e_1 - e_2)(S_{ix}^2 - S_{iy}^2)\Big]$$

$$+ g_3(e_4 S_{iy}S_{iz} + e_5 S_{ix}S_{iz} + e_6 S_{ix}S_{iy})\Big\},$$

$$H^{ee} = C_{11}(e_1^2 + e_2^2 + e_3^2) + C_{12}(e_1e_2 + e_2e_3 + e_3e_1)$$
$$+ C_{44}(e_4^2 + e_5^2 + e_6^2).$$

The elastic strains e_i are written in Voigt notation as

$$e_1 = u_{11}, \quad e_2 = u_{22}, \quad e_3 = u_{33},$$
$$e_4 = 2u_{23}, \quad e_5 = 2u_{13}, \quad e_6 = 2u_{12},$$
$$u_{ij} = (\partial u_i/\partial x_j + \partial u_j/\partial x_i)/2.$$

In order to find the numerical values of the coefficients in the effective Hamiltonian (5), we used the results of calculations of the lattice vibration spectrum and the total crystal energy for some low-symmetry phases whose distortions involve F-ion displacements.

The elastic constants C_{11}, C_{12}, and C_{44} are determined from the calculated small-q dependences of the frequencies of longitudinal and transverse acoustic modes for three symmetry directions: [001], [110], and [111]. The following values are obtained for the elastic constants $C_{ij} = c_{ij}\Omega$ (where Ω is the unit-cell volume) for the Rb_2KInF_6 crystal: $C_{11} = 53.6$ eV, $C_{12} = 11.7$ eV, and $C_{44} = 9.5$ eV. Unfortunately, experimental values of the elastic constants of this crystal are unavailable and we can only compare the calculated constants C_{ij} with their experimental values for the isomorphic compound Rb_2NaHoF_6, which has approximately the same chemical composition as the crystal under study: $C_{11} = 59.5$ eV, $C_{12} = 18.9$ eV, and $C_{44} = 19.2$ eV [15]. It is seen that these values and the respective constants calculated for the Rb_2KInF_6 crystal are of the same order of magnitude.

The coefficients of the second-order terms in Eq. (5) are determined from the total energies E_i of the distorted phases. Table 5 presents the relations between linear combinations of the coefficients in Eq. (5) and the distortion energies $\Delta E_i = E_i - E_0 - E_{anh}$ (where $E_0 = -356596$ eV), as well as the values of ΔE_i (in eV) calculated from first principles. In this table, E_Γ is the energy of the tetragonally distorted phase in which the rotations of InF_6 octahedra are homogeneous over the crystal and correspond to condensation of one compo-

Table 5. Expressions for the distortion energies $\Delta E_i = E_i - E_0 - E_{anh}$ of some phases and their values (eV)

ΔE_Γ	$4a_1 + 8a_2 + 2b_1 + 4b_2 + A$	–26.906
ΔE_X	$4a_1 - 8a_2 + 2b_1 + 4b_2 + A$	–26.169
ΔE_L	$-24a_3 - 6b_1 - 12b_2 + 3A$	18.412
ΔE_{zx}	$-4a_1 + 2b_1 + 4b_2 + A$	16.557

Table 6. Calculated phase transition temperatures (K) and the parameters of the effective Hamiltonian (eV)

T_c	550	750	450	350
Single-site parameters				
A	3.087	–15.482	23.490	5.339
B	1.400×10^3	1.577×10^3	1.188×10^3	1.286×10^3
C	2.246×10^3	2.145×10^3	2.415×10^3	2.767×10^3
D	-0.732×10^3	-5.568×10^3	5.567×10^3	16.198×10^3
Intersite parameters				
a_1	–5.386	–3.928	–7.785	–4.969
a_2	–0.046	–0.027	–0.073	0.060
a_3	0.628	0.514	0.849	0.014
b	–1.346	–0.982	–1.948	–1.243
Coupling constants with homogeneous strains				
g_1	39.878	66.420	43.430	29.854
g_2	–15.915	–15.939	–20.672	–18.701

nent of the T_{1g} mode at $q = 0$; E_X is the energy of the tetragonally distorted phase with a doubled unit-cell volume, resulting from condensation of the soft mode X_2^+ at the BZ boundary; and ΔE_L is the difference between the energies of the cubic and the distorted phase in which the octahedra are rotated about a cube body diagonal, which corresponds to the following distribution of the local mode $S_\alpha(\mathbf{R})$:

$$S_x(\mathbf{R}) = S_y(\mathbf{R}) = S_z(\mathbf{R}) = |S| \exp(-i\mathbf{q}_L\mathbf{R}),$$

where $|S|$ is the amplitude of the local mode, $\mathbf{q}_L = \frac{\pi}{a_0}(111)$, and $\mathbf{R}$ is a translation vector of the cubic phase. The amplitude of this local mode is found by minimizing the total energy E_L of the distorted phase. It should be noted that, although this distorted phase cannot result from the condensation of any one phonon mode, the crystal under study has an unstable mode at point L on the BZ boundary in which the displacements of the ions lead to rotation of the octahedron and to a small distortion in it [9]. We also calculated the total energy E_{zx} of the distorted phase in which the InF_6 octahedron is rotated about the [001] axis and the unit cell is doubled along the [100] axis, which corresponds to an $S_\alpha(\mathbf{R})$ distribution of the form

$$S_z(\mathbf{R}) = |S| \exp(-i\mathbf{q}_X\mathbf{R}), \quad S_x = S_y = 0,$$

where $\mathbf{q}_X = \frac{2\pi}{a_0}(100)$. This distorted structure cannot be due to the condensation of a phonon mode. Since the other homogeneously distorted structures in which the unit cell is doubled and the octahedra are rotated do not lead to new relations between linear combinations of the coefficients, we failed to divide the combination $4a_1 + 2b_1 + 4b_2 + A$ into individual terms. For this reason, we assumed that the constants b_1 and b_2, which characterize the interaction with the next-to-nearest neighbors in Eq. (5), have the same value and are four times less than the interaction constant with the nearest neighbors a_1; that is, $b_1 = b_2 = b = a_1/4$. This assumption is consistent with our calculations of the thermodynamic properties of the system with Hamiltonian (5) (see below), according to which these properties (calculated with the value of a_1 determined previously) are scarcely affected by the values of b_1 and b_2; at least, for three values of $b/a_1 = 1/4$, 1/2, and 3/4, the results of numerical simulations differ from one another only slightly.

The coefficients B, C, and D of the anharmonic terms in the single-site potential are determined from the dependences of the total energy of the clamped crystal (whose lattice parameter is the same as that in the cubic phase, $a_0 = 16.71$ a.u.) on the rotation angle of the InF_6 octahedron about the [001] ($S_x = S_y = 0$, $S_z = |S|$), [110] ($S_x = S_y = |S|$, $S_z = 0$), and [111] axes ($S_x = S_y = S_z = |S|$). These dependences are shown in Fig. 3, and the values of the coefficients B, C, and D determined using the least square method are listed in Table 6.

Now, we discuss the coupling coefficients between the local mode and homogeneous elastic strains. Since shear strains do not arise in the tetragonal phase during the $Fm3m \longrightarrow I4/m$ phase transition, we did not determine the coefficient g_3 in Eq. (5). The coefficients g_1 and g_2 are found as follows. The total energy of the unclamped crystal is calculated as a function of the rotation angle of the octahedron about the [001] axis and, for a fixed value of the angle, is minimized with respect to the unit-cell parameters and the radii of the Watson spheres of the ions. The angular dependence of the energy is shown in Fig. 3. Then, we subtract the total energy of the clamped crystal, and this energy difference and the elastic constants determined before are used to fit the coefficients g_1 and g_2 using the least square method (Fig. 3). The values of these coefficients are listed in Table 6.

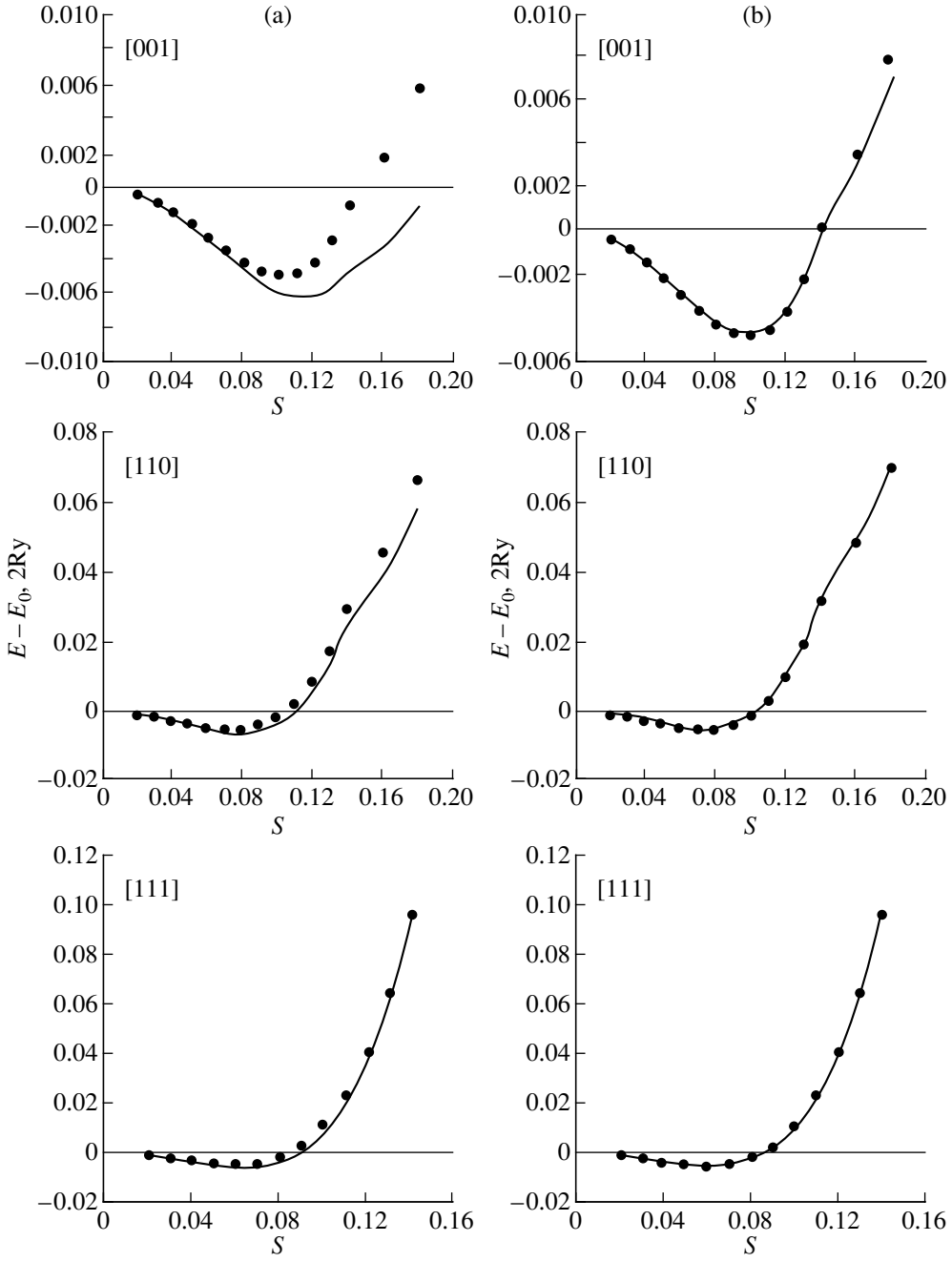

Fig. 3. Total crystal energy (E_0 = –13110.141187 a.u.) as a function of the octahedron rotation angle for (a) the unclamped crystal and (b) the clamped crystal with unit-cell parameters of the cubic phase. Solid curves are calculations, and dots represent the energies obtained from the effective Hamiltonian, whose parameters are fitted using the least square method.

5. INVESTIGATION OF THERMODYNAMIC PROPERTIES AND DISCUSSION OF RESULTS

The effective Hamiltonian derived above is simple but contains many parameters, which hampers calculation of the free energy and other thermodynamic quantities using analytical methods, for example, within the self-consistent-field approximation. Therefore, we investigated the thermodynamic properties of the system with the effective Hamiltonian (5) using the numerical Monte Carlo (MC) method, namely, its classical version with the Metropolis algorithm [16] for an fcc $L \times L \times L$ lattice with periodic boundary conditions. The three-component pseudovector (S_x, S_y, S_z) was placed at each lattice site, and the lattice was subjected to homogeneous strains e_1, e_2, and e_3. We investigated two cases using the MC method: a clamped crystal (i.e., without elastic strains, $e_1 = e_2 = e_3 = 0$) and an unclamped crystal with strains e_1, e_2, and e_3 (their cal-

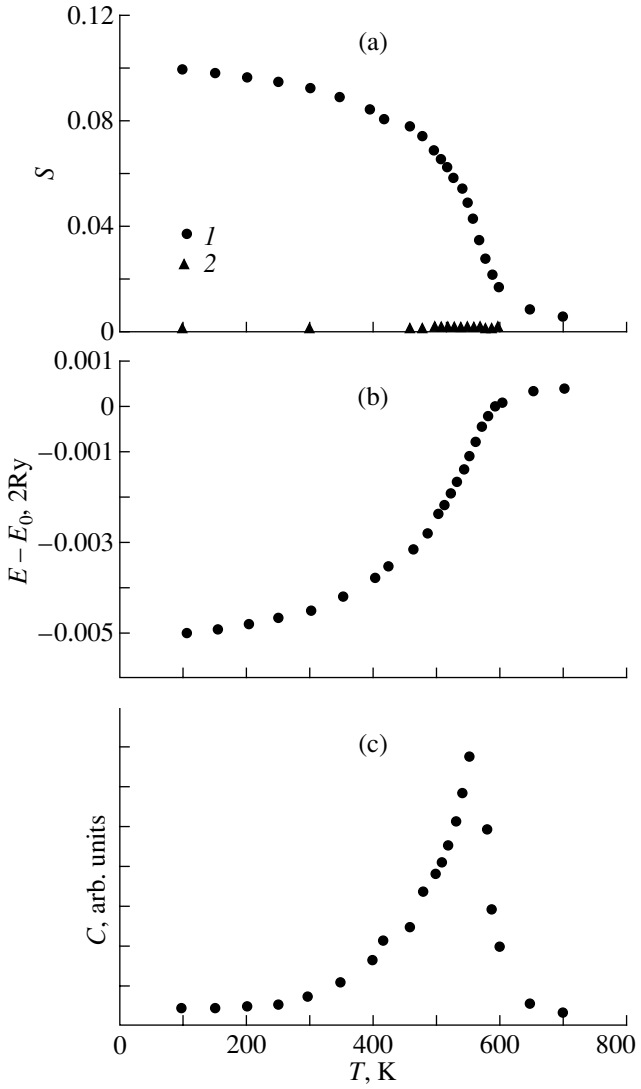

Fig. 4. Temperature dependences, calculated using the MC method, of (a) the order parameter (*1* is S_z, *2* is S_x, S_y), (b) the internal energy, and (c) the heat capacity (in arbitrary units).

culation was included in the MC algorithm). In the former case, in each cycle of the MC procedure, we varied the pseudovector components S_{ix}, S_{iy}, and S_{iz} in a random fashion successively at each lattice site and verified the possibility of each variation. It should be noted here that our calculations of the total energy of distorted phases and numerical simulations of the effective Hamiltonian showed that the energies of distorted phases with unequal pseudovector components $S_x \neq S_y \neq S_z$ were significantly higher than those in the case of equal pseudovector components. Therefore, in order to reduce the computer time required for the MC procedure, we chose only those pseudovectors with the following components: S_z, $S_x = S_y = 0$; $S_z = \pm S_x$, $S_y = 0$; and $S_z = \pm S_x = \pm S_y$.

Since the energy increases sharply in the range above $|S| \sim 0.07$, as seen from Fig. 3, we restricted our calculations to the range [–0.1, 0.1] for the values of the components S_α and their variations. For each value of the temperature, we performed 50000 steps of the MC procedure and the thermodynamic quantities were calculated by averaging over the last 10000 steps in the ordinary way [16].

In the case of the unclamped crystal, after each cycle of the MC procedure described above, we tried to vary each component of the strain tensor. The values of trial variations were chosen randomly and lied in the range [–0.05, 0.05]. For each component, we performed 1000 trials and averaged over them. The averaged strains and the configuration of pseudovectors calculated in a given cycle of the MC procedure were taken as the initial ones for the next cycle.

The calculations were carried out for both high (~1000 K) and low (~50 K) initial temperatures. When the MC procedure was started from high temperatures, we simultaneously treated two initial configurations, corresponding to the high-symmetry cubic phase ($S_x^i = S_y^i = S_z^i = 0$) and to the tetragonally distorted phase ($S_z^i = 0.08$, $S_x^i = S_y^i = 0$). When starting from low temperatures, a configuration corresponding to the tetragonal phase was taken as the initial one. The calculation was carried out for the dimension $L = 10$ (4000 pseudovectors). In order to check the results, we also performed calculations for several temperatures for a larger lattice ($L = 20$, 32000 pseudovectors). The results obtained for the $20 \times 20 \times 20$ lattice differ little from those obtained for the $10 \times 10 \times 10$ lattice; thus, in what follows, we will discuss only the calculations performed for $L = 10$.

The calculated temperature dependences of the pseudovector components S_x^i, S_y^i, and S_z^i and of the internal energy $E - E_0$ (E_0 is the total energy of the crystal in the cubic phase) are shown in Fig. 4. The phase transition temperature was determined as that corresponding to the inflection point in the temperature dependence of the internal energy (Fig. 4b) and to the peak in the temperature dependence of the heat capacity C_V calculated using a standard method [16] (Fig. 4c).

At $T_c = 550$ K, the unclamped crystal undergoes a second-order phase transition to a distorted phase with pseudovectors $S_z^i = S$ and $S_x^i = S_y^i = 0$. Such a tetragonal phase, having the same unit-cell volume as the cubic phase and belonging to the space group $I4/m$, was observed experimentally in Rb_2KInF_6 crystals below 283 K [5]. The calculation accuracy of the phase transition temperature is determined by that of the vibration frequencies and of the total energy of the distorted phases. In the approach employed by us, these quantities are calculated to within an accuracy of ~5%. In the

case of the clamped crystal (zero strains), the phase transition temperature obtained from the MC calculation data is T_c = 560 K, which is ten degrees higher than that for the unclamped crystal.

Figure 5 presents the elastic strains $e_1 = e_2$ and e_3 in the tetragonal phase measured experimentally and from MC calculations. The quantitative agreement between the calculated and experimental values is fairly reasonable, if one takes into account that the values of e_i are very small and that the method according to which we calculated the total crystal energy, vibration frequencies, and the parameters of the model Hamiltonian is poorly accurate.

The phase transition temperature T_c obtained from the MC calculations is nearly twice as large as its experimental value. This discrepancy can be mainly due to the calculated total crystal energy and lattice vibration spectrum, which are not sufficiently accurate in comparison with the first-principles energy-band calculations.

On the other hand, our calculations revealed that the value of the phase transition temperature is very sensitive to the details of the crystal structure in both the high-symmetry cubic phase and the distorted phases. The parameters of the effective Hamiltonian (5) listed in the second column of Table 6 were calculated from the energies of the distorted phases by minimizing the total crystal energy in both the cubic and distorted phases. We also calculated the parameters of the effective Hamiltonian (by following the scheme described above) and performed MC calculations with these parameters for slightly varied crystal structures. The results of these calculations are presented in the last three columns of Table 6: The third column lists the parameters of the Hamiltonian and the calculated phase transition temperature for the case where the F–In distance (between the fluorine and indium ions) in the cubic phase is $0.222a_0$ (a_0 = 17.08 a.u. is the lattice parameter in the cubic phase), the fourth column lists the same quantities calculated for a F–In distance equal to $0.24a_0$ (a_0 = 16.41 a.u.), and the last column of Table 6 lists the same quantities calculated for the case where the F–In distance ($0.23a_0$, a_0 = 16.71 a.u.) corresponds to the minimum of the total energy but, in addition to the F-ion displacements, the Rb ions in the tetragonally distorted phase are also displaced along the cube body diagonal without breaking the tetragonal symmetry. The amount of Rb-ion displacement was taken to be equal to one-third the F-ion displacement. It can be seen from Table 6 that small variations (≈4%) of the ion positions in the crystal structure give rise to significant changes in T_c. However, it should be emphasized once again that the values of the transition temperature from the cubic to the tetragonal phase listed in the last three columns of Table 6 do not correspond to a minimum of the total crystal energy.

According to our MC calculations, the tetragonal phase remains stable down to zero temperature and the other pseudovector components (S_x, S_y) do not appear, which contradicts the experimental observations, according to which another structural phase transition (to the monoclinic phase with unit-cell doubling) occurs in Rb_2KInF_6 crystals at T_{c2} = 264 K. Structural studies of the monoclinic phase of the isomorphic Rb_2KScF_6 compound revealed [5] that this phase transition is accompanied by the appearance of another pseudovector component below T_{c2}; this component is inhomogeneous over the crystal and involves displacements of the Rb ions from their equilibrium positions. This suggests that the Rb-ion displacements play a significant part in the stabilization of the monoclinic phase in this crystal and that, therefore, in order to describe the second structural phase transition, not only octahedron rotations but also the vibrational modes that correspond to these degrees of freedom should be included into the model Hamiltonian.

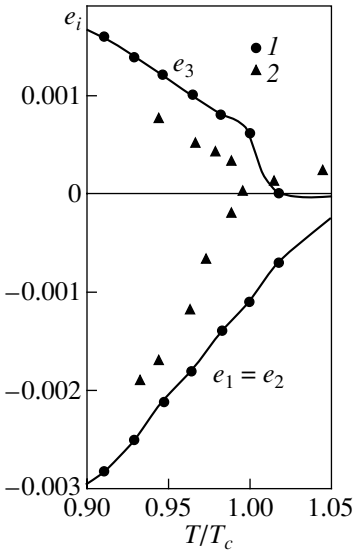

Fig. 5. Temperature dependences of the strain tensor components e_i in the tetragonal phase: (*1*) MC calculations and (*2*) experiment [17].

6. CONCLUSIONS

Thus, in this paper, we calculated the entire spectrum of crystal lattice vibrations and constructed a nonempirical effective Hamiltonian to describe the structural phase transition $Fm3m \longrightarrow I4/m$ in the Rb_2KInF_6 crystal. The parameters of the Hamiltonian were determined by calculating the total energy in an ionic-crystal model taking into account the deformation and polarization of ions. The model Hamiltonian was used in numerical calculations in accordance with the MC method, from which we determined the phase transition temperature from the cubic to the tetragonal phase, T_c = 550 K. This calculated temperature is twice as large as the corresponding experimental value. This discrepancy could be mainly due to the insufficiently accurate

method used in the calculations. However, according to our calculations, the phase transition temperature is very sensitive to the details of the crystal structure; therefore, the discrepancy between the calculated and experimental values of T_c could be due to the imperfection of the crystals used in the experimental studies.

Nevertheless, from the results obtained in this paper, it is reasonable to infer that the phase transition $Fm3m \longrightarrow I4/m$ in the Rb_2KInF_6 crystal is basically associated with spatially homogeneous rotations of the InF_6 octahedra, whereas the other degrees of freedom affect the mechanism and thermodynamics of this phase transition only slightly.

ACKNOWLEDGMENTS

The authors are grateful to O.V. Ivanov and E.G. Maksimov for permission to employ the computer code for calculating the total crystal energy and ionic polarizability.

This study was supported by the Russian Foundation for Basic Research, project nos. 00-02-17792, 00-15-96790, and the INTAS Foundation, grant no. 97-10-177.

REFERENCES

1. R. D. King-Smith and D. Vanderbilt, Phys. Rev. B **49**, 5828 (1994).
2. K. M. Rabe and U. V. Waghmare, Ferroelectrics **164**, 15 (1995).
3. U. V. Waghmare and K. M. Rabe, Phys. Rev. B **55**, 6161 (1997).
4. D. Vanderbilt and W. Zhong, Ferroelectrics **206** (1–4), 181 (1998); W. Zhong, D. Vanderbilt, and K. M. Rabe, Phys. Rev. B **52**, 6301 (1995).
5. I. N. Flerov, M. V. Gorev, K. S. Aleksandrov, *et al.*, Mater. Sci. Eng., R **24**, 81 (1998).
6. V. I. Zinenko and N. G. Zamkova, Fiz. Tverd. Tela (St. Petersburg) **41**, 1297 (1999) [Phys. Solid State **41**, 1185 (1999)].
7. O. V. Ivanov and E. G. Maksimov, Zh. Éksp. Teor. Fiz. **108**, 1841 (1995) [JETP **81**, 1008 (1995)].
8. V. I. Zinenko and N. G. Zamkova, Zh. Éksp. Teor. Fiz. **118** (2), 359 (2000) [JETP **91**, 314 (2000)].
9. V. I. Zinenko, N. G. Zamkova, and S. N. Sofronova, Zh. Éksp. Teor. Fiz. **114** (5), 1742 (1998) [JETP **87**, 944 (1998)].
10. D. A. Liberman, D. T. Cromer, and J. J. Waber, Comput. Phys. Commun. **2**, 107 (1971).
11. H. Guengard, Ph.D. Thesis (University of Bordeaux, France, 1994).
12. M. Couzi, S. Khairoun, and A. Tressaud, Phys. Status Solidi A **98**, 423 (1986).
13. H. Thomas and K. A. Muller, Phys. Rev. Lett. **21**, 1256 (1968).
14. K. M. Rabe and J. D. Joannopoloulos, Phys. Rev. B **36**, 6631 (1987).
15. P. Selgert, C. Lingner, and B. Luthi, Z. Phys. B **55**, 219 (1984).
16. *Monte Carlo Methods in Statistical Physics*, Ed. by K. Binder (Springer, Berlin, 1979; Mir, Moscow, 1982).
17. I. N. Flerov, M. V. Gorev, S. V. Mel'nikova, *et al.*, Fiz. Tverd. Tela (St. Petersburg) **34**, 3493 (1992) [Sov. Phys. Solid State **34**, 1870 (1992)].

Translated by Yu. Epifanov